Available online at www.sciencedirect.com
SCIENCE DIRECT®
Microporous and Mesoporous Materials 71 (2004) 185–198
MICROPOROUS AND MESOPOROUS MATERIALS
www.elsevier.com/locate/micromeso

Se incorporated into zeolite mordenite-Na: a single-crystal X-ray study

Petra Simoncic, Thomas Armbruster *

Laboratorium für Chemische und Mineralogische Kristallographie, University of Bern, Freiestrasse 3, CH-3012 Bern, Switzerland

Received 9 February 2004; received in revised form 24 March 2004; accepted 29 March 2004

Abstract

Single crystals of self-synthesized mordenite-Na were used for incorporation of elemental selenium. The mordenite sample was first dehydrated at 280 °C and selenium was subsequently incorporated as gas phase at 450 °C for 72 h. Bright orange-colored Se-loaded mordenite was quantitatively analyzed by an electron microprobe yielding $Na_6Al_6Si_{42}O_{96} \cdot [Se_{7.9}]$. X-ray data collection of mordenite-Na and Se-loaded mordenite-Na single-crystals were performed at 120 K with synchrotron radiation ($\lambda = 0.79946$ Å) using the single-crystal diffraction line at SNBL (ESRF, Grenoble), where diffracted intensities were registered with a MAR image plate. The structures of mordenite-Na and Se-mordenite-Na were both refined in the monoclinic space group *Cc* converging at $R1 = 5.25\%$ (mordenite-Na), and $R1 = 6.65\%$ (Se-mordenite-Na). A strongly broadened Raman band at approximately 254 cm^{-1} confirmed the existence of Se chains in the 12-membered channels along the *c*-axis. Several, low-populated, disordered Se chains with a length up to 10 Å and seven Se atoms were located in the large mordenite channels. During structure refinement nearest and next nearest neighbor Se–Se distances were fixed at 2.34 and 3.62 Å, respectively. Other distances and angles remained unconstrained. Because of electrostatic interaction with the framework and influence of extraframework occupants such as Na^+ and H_2O molecules, the chains show different geometrical Se arrangement with highly variable dihedral angles. Any other Se species such as Se_6 or Se_8 rings were neither confirmed by structure refinement nor by Raman spectroscopy. There was no indication of a trigonal Se chain geometry within the 12-membered ring channel.

Keywords: Zeolites; Mordenite; Single-crystal X-ray study; Semiconductor material; Selenium

1. Introduction

Microporous materials as zeolites are more and more applied for the design and development of new materials. With their channels and cavities of several angstroms in size, they allow a spatial arrangement and stabilization of individual atoms, clusters or molecules. One aspect of modern technology and new materials are one-dimensional systems and miniaturized electronic devices with fast response, high selectivity, and efficiency, e.g. semiconductors organized as quantum dots or chains in zeolites channels. Semiconductor materials were encapsulated in synthetic zeolites such as $AlPO_4$-5, zeolites A and Y [1–3] with their uniform and large channels (>7 Å), but also the naturally occurring mordenite with its compressed channels (7×6.5 Å) was successfully used for molecular organization of atoms and molecules.

The structure of mordenite can be described as built by edge-sharing 5-membered rings of tetrahedra (secondary building unit 5-1) forming chains along the *c*-axis [4]. However, the mordenite framework can also be more comprehensibly envisioned as formed by puckered sheets parallel to (1 0 0), assembled of 6-membered rings of tetrahedra [5,6]. These sheets are interlinked by 4-membered rings (Fig. 1) in a way that large, ellipsoidal 12-membered (12MR*c*: aperture 7×6.5 Å) and strongly compressed 8-membered rings (8MR*c*: aperture 5.7×2.6 Å) define channels parallel to the *c*-axis. Another set of compressed 8-membered rings (8MR*b*: aperture 3.4×4.8 Å) connects the wide channels with the strongly compressed channels parallel to the *b*-axis.

Elemental selenium incorporated into mordenite is a good example of a one-dimensional semiconductor and

* Corresponding author. Fax: +41-31-631-3996.
E-mail address: thomas.armbruster@krist.unibe.ch (T. Armbruster).

1387-1811/$ - see front matter © 2004 Published by Elsevier Inc.
doi:10.1016/j.micromeso.2004.03.031

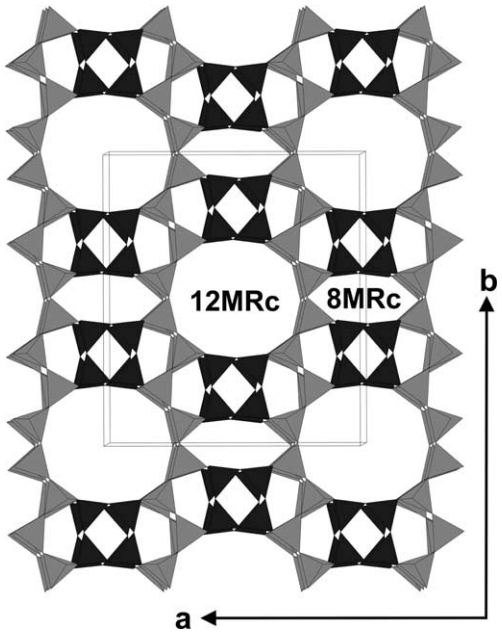

Fig. 1. Tetrahedral framework structure of mordenite with unit-cell outlines. The structure can be envisioned as built by puckered sheets (light gray shading) parallel to (1 0 0) formed by 6-membered rings of tetrahedra. These sheets are connected along *a* by 4-membered ring pillars (dark gray shading) in a way that 12-memebered ring channels (12MR*c*) and compressed 8-membered ring channels (8MR*c*) are formed, both extending along *c*.

this host–guest system has widely been investigated. Two methods have been established for encapsulation of Se in mordenite: (1) adsorption in gas phase and (2) molten selenium injection under pressure. Elemental selenium exists in different solid modification: two monoclinic, both characterized by Se_8 rings, a trigonal, an amorphous, and a cubic modification. The trigonal phase is the only stable phase under ambient conditions. The trigonal Se modification builds helical chains. Typical bond lengths to nearest and next nearest neighbors are 2.373(5) and 3.72 Å, respectively. The Se–Se–Se bond angle is $103° \pm 0.02$ [7].

The channel wall, as well as extraframework cations and H_2O molecules affect Se incorporated into mordenite. Therefore, it can be expected that the form of a helical chain will be influenced by the zeolite structure and symmetry and will be different to the trigonal helical chain known from the Se polytype. Structure and arrangement of Se atoms in zeolites were mainly investigated by Raman spectroscopy, X-ray adsorption, EXAFS, XANES and electron microscopy where helical Se chains and their forms were verified in mordenite channels.

A slightly inclined selenium chain within the large channels of mordenite along *c* is composed of approximately six Se atoms yielding the periodicity of the mordenite *c* translation (7.5 Å). Thus, if the channels are completely occupied by Se chains, the maximum Se concentrations amounts to approximately 12 Se per formula unit (p.f.u.).

First experiments concerning elemental Se in mordenite were done by Bogomolov et al. [8]. They incorporated Se and Te by gas phase as well as by injection from Se melt under pressure and reported optical density spectra of Se- and Te-mordenite. They postulated that the symmetry of the chains in the mordenite channels differs from the symmetry of elemental Se and Te (D_3), due to variation of the dihedral angle but with constant bond length and bond angle. In a second study, Bogomolov et al. [9] compared Raman spectra of trigonal and monoclinic Se with those of Se incorporated into mordenite. They observed a clear shift of the Raman active A1 symmetric stretching mode to higher frequency for Se in mordenite. Due to similar modes in Se-mordenite compared with the symmetric bond-bending modes of Se_8, they proposed ring- and chain-like Se fragments in the mordenite channel distinct by variation of the dihedral angle. They expected that the dihedral angle could deviate up to 30° from the preferred value of 102°.

Poborchii and co-authors performed series of experiments [10–15] with Se loaded in different zeolites (mordenite, cancrinite, $AlPO_4$-5) applying EXAFS and Raman spectroscopy. They discussed the influence of ion exchange and different incorporation methods of Se in mordenite on the form of the Se in the channels. Poborchii and co-authors [10–15] observed that Se chains are more regular if Se is incorporated by vapor adsorption. In addition to Se chains, they postulated also 6-membered Se rings located in the mordenite channel. The relative concentration of rings or chains is not dependent of the incorporation method but of type of extraframework cations in mordenite. The Se chain concentration is decreasing compared to Se_6-rings and Se–Se bond lengths increase if extraframework Na-ions are substituted by other monovalent cations. Poborchii [10] discussed also the geometry of Se chains. Based on the work of Bogolomov et al. [8,9], Poborchii derived a Se chain arrangement in the mordenite channel from stretching and bending modes of Raman spectra.

Terasaki et al. [16] performed an electron microscopy study on synthetic H^+-exchanged mordenite, modified with vapor-induced Se. High-resolution images showed that channels are patch-wise filled with selenium.

Based on EXAFS experiments, bond lengths and angles of Se chains in mordenite were discussed by Khouchaf et al. [17], Parise et al. [18] and Katayama et al. [19]. The nearest neighbor distance between Se atoms was determined by all groups to 2.34 Å, next nearest neighbor distance to 3.62 Å with a bond angle of 102°. Nearest and next nearest distances of Se atoms in mordenite are therefore shorter than in trigonal Se. The third neighbor distance was more difficult to determine. Khouchaf et al. [17] and Katayama et al. [19] derived from EXAFS data a corresponding distance of 4.3 Å.

This distance was assumed [17] to be due to an overlap of two chains (interchain distance), whereas Katayama et al. [19] interpreted it as an intrachain distance to the third neighbor. Thus the details of the third neighbor distance, which is crucial for the form of the Se chain in mordenite, remained unclear.

Ikawa and Fukutome [20,21] calculated semiempirical models for the electronic and lattice structure of isolated Se chains in mordenite channels and discussed internal defects of Se chains and interactions with cations, H_2O molecules, and framework oxygen. They postulated that incorporated Se is highly influenced by the zeolite host. The modeled chains show different geometries due to variation of the dihedral angle, which are distinct from the trigonal Se chains.

Whereas the existence of rings and chains in mordenite channels is confirmed by different spectroscopic methods, the exact structure of encapsulated Se has not been solved yet. In particular, the form of Se chains is controversially discussed. Single-crystal X-ray diffraction is a suitable method for investigating Se-modified mordenite. The aims of this study are (1) incorporation of Se in self-synthesized, large mordenite single-crystals; (2) study of location and bonding of Se in mordenite channels by single-crystal X-ray diffraction.

2. Experimental

2.1. Sample

Pure mordenite-Na crystals were synthesized hydrothermally in the home lab after a modified method by Warzywoda et al. [22]. The exact synthesis conditions are summarized in Table 1. The crystallization products were 100% mordenite with platy and uniform morphology. The run products were studied with a polarizing microscope and the single crystals were examined with a scanning electron microscope and showed well-defined, but slightly curved faces and no apparent twinning. Average size of the mordenite crystals was about $0.06\times0.04\times0.05$ mm (Fig. 2). Previous ion-exchange experiments with cationic dyes [23] showed that the used sample is a large port mordenite, and therefore suitable for incorporation of Se chains.

Table 1
Synthesis conditions for mordenite single-crystals

Mordenite
Batch composition $4.32Na_2O$, $19SiO_2$, $1Al_2O_3$, $293.6H_2O$
Source materials Distilled water Sodium hydroxide (Hänseler) Sodium aluminate (Riedel-de Haen, anhydrous, technical) Silica gel (Aldrich, grade 62, 60–200 mesh, 150 Å; preheated 24 h at 850 °C under air) Ethanol
Batch preparation (1) [0.1858 g sodium hydroxide + 1.8277 g distilled water], stir until dissolved (2) [0.1147 g sodium aluminate and 1.8277 g distilled water], stir until dissolved (3) [(1) + (2) + 0.7989 g preheated silica gel + 2 ml ethanol], mix and stir for 30 min
Crystallization Teflon autoclave, 50 ml Temperature, 175 °C Time, 96 h
Product recovery (1) Filter and wash < pH 10 (2) Dry at 100 °C
Reference Warzywoda et al. [22]

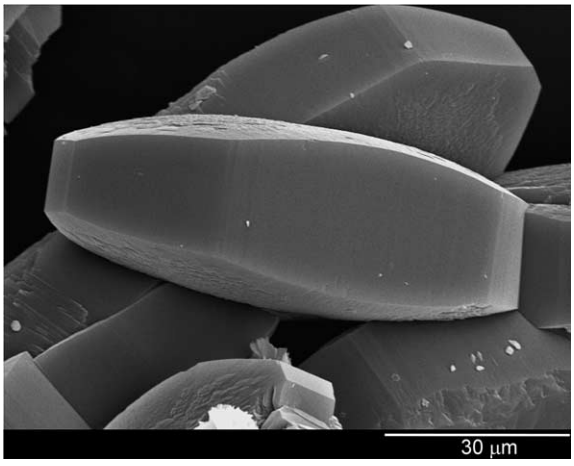

Fig. 2. Scanning electron microscopic image of synthetic, platy mordenite of $Na_6Al_{6.02}Si_{42.02}O_{96}\cdot 19H_2O$ composition. Notice that the (0 0 1) face is rough and slightly curved. The large channels (Fig. 1) run perpendicular to this face.

2.2. Selenium incorporation

Self-synthesized mordenite-Na was used for encapsulation of elemental selenium. Mordenite single-crystals (≈5 mg) were dehydrated at 280 °C in an open glass tube (0.3 ml, outer diameter: 5 mm, wall thickness: 1 mm) for 2 h. Previous thermo-gravimetric (TG) analysis showed that mordenite-Na is completely dehydrated after this treatment and no extraframework H_2O is present in mordenite-Na before Se incorporation. After dehydration the temperature was rapidly lowered to 150 °C and approximately 10 mg Se (Aldrich, 99.5%) was added into the glass tube, which was immediately sealed. The sealed tube was subsequently heated in an oven at 450 °C for 72 h and then cooled down in the oven to room temperature. The crystals were examined under an optical microscope showing a clear pleochroism changing from orange to yellow. Successful incorporation was

also confirmed by Raman spectroscopy performed on a RamSpec spectrometer using a laser with 532.12 nm wavelength attached to an optical polarizing microscope, which enables single-crystal studies (Fig. 3). Se-loaded mordenite was quantitatively determined by electron microprobe analyses resulting in a chemical composition of $Na_6Al_6Si_{42}O_{96} \cdot [Se_{7.9}] \cdot nH_2O$. Electron microprobe analysis showed also that Se is uniformly incorporated into mordenite; no zoning was detected.

2.3. X-ray data collection

X-ray data collection of synthetic mordenite-Na (as synthesized) and Se-treated (Se-mordenite-Na) single crystals were performed at 120 K using a conventional liquid-N_2 device with synchrotron radiation (wavelength $\lambda = 0.79946$ Å) on the single-crystal diffraction line at SNBL (ESRF, Grenoble), where diffracted intensities were registered with a MAR image plate. The double experiments were performed to detect possible phase transitions in the mordenite structure at low temperature due to the influence of Se incorporation. The reason for intensity data collection at low temperature was to reduce thermal vibration of extraframework Se in order to allow more accurate localization. Data reduction was performed with the program package CrysAlis [24] and an empirical absorption correction was made with SADABS [25]. A summary of experimental parameters is given in Table 2.

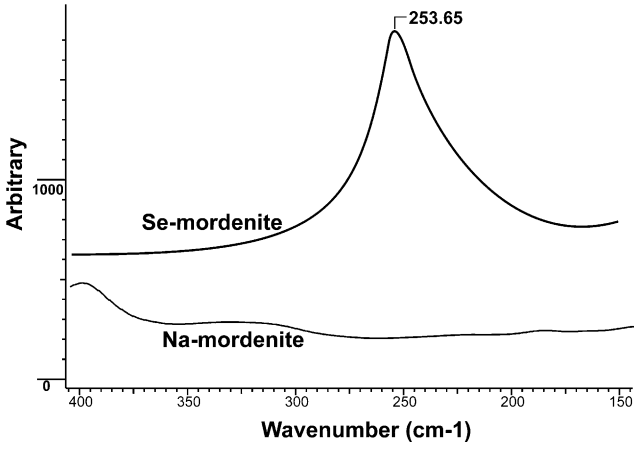

Fig. 3. Raman spectrum from 150 to 400 cm^{-1} of Se-mordenite-Na and mordenite-Na. A dominant vibration band at 253.65 cm^{-1} in Se-mordenite-Na is absent in mordenite-Na. According to literature data [9–15], this band can be attributed to the symmetric stretching band A1 in a Se chain.

Structure refinement for mordenite-Na and Se-mordenite-Na was carried out with the program SHELXL97 [26], using neutral-atom scattering factors (Si for all tetrahedral sites—labeled T sites). Refinements were performed with anisotropic displacement parameters for all framework sites and highly populated extraframework positions. Test refinements were carried out in space groups *Cmcm*, $Cmc2_1$, $C2/c$ and *Cc*. Final data were presented in space group *Cc* for both structures. In addition, a *c*/2-shifted defect domain was introduced and fully constrained to the Si/Al framework [27]. The O8 site was split into four isotropic satellite positions, which were approximately equally occupied. Na- and H_2O positions were determined by comparison with diffraction data of synthetic mordenite at room temperature [27].

Se sites were identified by analyzing difference Fourier maps focusing on the 12-membered ring channel of mordenite-Na and Se-mordenite-Na. Clear differences

Table 2
Experimental parameters for X-ray data collection and refinement of mordenite-Na and Se-mordenite-Na

Sample	Mordenite-Na	Se-Mordenite-Na
Crystal size (mm)	0.05×0.04×0.50	0.06×0.04×0.05
Diffractometer	Mar image plate	Mar image plate
X-ray radiation	Synchrotron (0.7995 Å)	Synchrotron (0.7995 Å)
Temperature	120 K	120 K
Space group	*Cc*	*Cc*
Cell dimensions$_{a,b,c}$ (Å)	18.073(3), 20.463(3), 7.5145(9)	18.077(3), 20.509(2), 7.5172(9)
β (°)	90.05(1)	90.03(2)
Absorption corr.	SADABS	SADABS
Maximum 2θ	48.59	48.55
Measured reflections	15,595	15,670
Index range	$-20 \leqslant h \leqslant 20$, $-23 \leqslant k \leqslant 23$, $-8 \leqslant l \leqslant 8$	$-20 \leqslant h \leqslant 20$, $-23 \leqslant k \leqslant 23$, $-8 \leqslant l \leqslant 8$
Unique reflections	4468	4440
Reflections > $4\sigma(F_0)$	4180	4212
R_{int}	0.0347	0.0355
R_σ	0.0398	0.0317
Number of l.s. parameters	362	359
GooF	1.131	1.096
R1, $F_0 > 4\sigma(F_0)$	0.0525	0.0665
R1, all data	0.0573	0.0700
WR2 (on F_0^2)	0.1095	0.1517

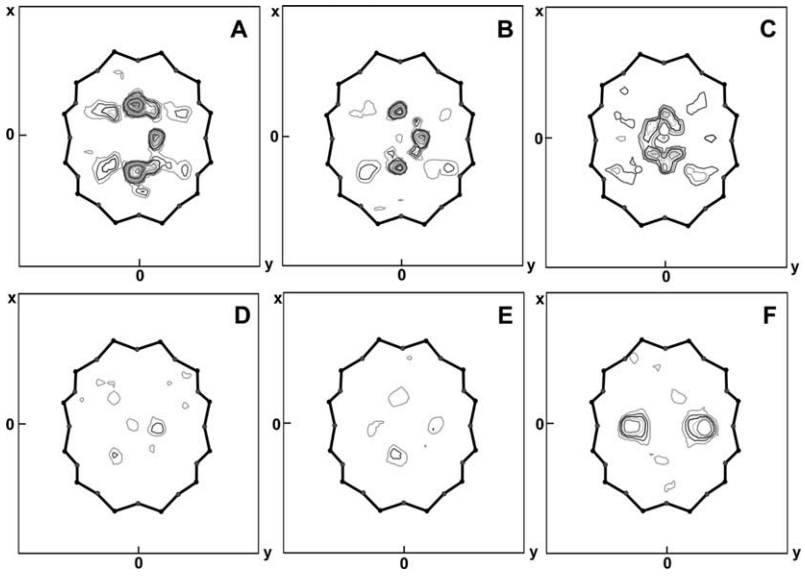

Fig. 4. Difference Fourier maps of Se-mordenite-Na and mordenite-Na, contours at 0.25 electron interval for all maps. Upper line Se-mordenite-Na—(A) (0 0 1) section of 12-membered ring channel at $z = -0.64$: Strong peaks shifted $\pm x$ from the center of the channel, as well as one strong peak shifted $+y$ from the center. (B) (0 0 1) section at $z = -0.51$: Strong peaks shifted $\pm x$ and $+y$ from the channel center. (C) (0 0 1) section at $z = -0.38$: strong, smeared electron density rhombus like around the center. Lower line mordenite-Na—(D) (0 0 1) section of 12-membered ring channel at $z = -0.64$ and (E) (0 0 1) section at $z = -0.51$: only weak electron density inside the channel. (F) (0 0 1) section at −0.38: Two peaks shifted $\pm y$ from the center, attributed to Na3.

of electron density in the channels are visible (Fig. 4). High electron density (3–5 e/Å^3) in the 12-membered ring channel of the Se-mordenite-Na is concentrated around the channel center, whereas only low electron density occurs in the corresponding mordenite-Na channel.

3. Results

3.1. Structure refinements

The single-crystal X-ray diffraction pattern of mordenite-Na and Se-treated mordenite-Na exhibited no difference concerning diffuse scattering features. In particular, there were no indications for super-structure reflections in the Se-treated mordenite-Na. The cell dimensions of both samples are very similar (Table 2) and the Se-treated crystal displayed only a significant expansion (0.2%) along the *b*-axis, the direction where the large channel with elliptical cross section is oblate.

The results of the structure refinement, comprising atomic coordinates, populations, and isotropic displacement parameters are given in Table 3 for Se-mordenite-Na. Atomic coordinates, populations and isotropic displacement parameters of the mordenite-Na framework are identical within two standard deviations, and therefore not displayed. Both samples show within two standard deviations the same mean T–O bond lengths (Tables 4 and 5). Mean T–O distances vary between 1.596 for T2c–O and 1.640 for T3a–O. Shortest bond lengths are in both samples around T2a–d. No estimations were made about Si/Al ordering, but based on T–O bond lengths a slight Al enrichment is assumed for tetrahedra in the 4-membered rings (T3 and T4), which is in agreement with literature data [27,28].

In mordenite-Na four Na sites were located, whereas in Se-mordenite-Na only three sites were found. Highest occupied Na1 (2.64 p.f.u. in Se-mordenite-Na, 2.32 p.f.u. in mordenite-Na) is situated in the center of the compressed 8-membered ring channel along *c*. Na2 is located at the intersection of the large 12-membered ring channel along *c* to the 8-membered ring channel along *b*. Na2 in the Se-mordenite-Na is occupied with 2.28 p.f.u., whereas the Na2 site in mordenite-Na was split in two satellite positions Na2a (0.52 p.f.u.) and Na2b (0.76 p.f.u.). The third Na site is located in the 12-membered ring channel but shifted from the center along *b*. Na3 in Se-mordenite-Na has the lowest occupation with 1.76 p.f.u. In mordenite-Na this site is also split in two satellite positions Na3a (1.36 p.f.u.) and Na3b (1.16 p.f.u.). In mordenite-Na, another site (Na4) is located in the center of the 12-membered ring channel along *c*, which is missing in the Se-mordenite-Na. Comparing extraframework cation distributions in synthetic mordenite-Na at room temperature [27] and 120 K, positions and occupations of the other Na sites are almost identical, whereas the Na3 site in low-temperature mordenite is slightly higher occupied than at room temperature. By comparison of the extraframework cation distribution in Se-mordenite-Na and mordenite-Na, it is obvious that the Na2 site in Se-mordenite-Na is higher occupied than

Table 3
Atomic coordinates and B_{eq} values for synthetic Se-mordenite-Na (space group *Cc*)

Atom	Population	*x*	*y*	*z*	B_{eq} [Å^2]
T1a	0.970(1)	0.30252(4)[1]	0.07286(9)[2]	0.1683(3)[3]	1.03(3)
T1b	0.970(1)	0.30252(4)[1]	−0.07286(9)[2]	0.0835(6)	1.03(3)
T1c	0.970(1)	−0.30252(4)[1]	0.07286(9)[2]	0.1683(3)[3]	1.11(4)
T1d	0.970(1)	−0.30252(4)[1]	−0.07286(9)[2]	0.0837(3)	1.11(4)
T2a	0.970(1)	0.19671(4)[4]	0.19037(9)[5]	0.6698(4)	1.11(3)
T2b	0.970(1)	0.19671(4)[4]	0.19037(9)[5]	0.0789(3)[6]	1.11(3)
T2c	0.970(1)	−0.19671(4)[4]	0.19037(9)[5]	−0.3304(3)	1.18(4)
T2d	0.970(1)	−0.19671(4)[4]	0.19037(9)[5]	0.0789(3)[6]	1.18(4)
T3a	0.970(1)	0.4132(2)	−0.11776(5)[7]	0.3743(4)[8]	1.10(3)
T3b	0.970(1)	−0.4122(2)	−0.11776(5)[7]	0.3743(4)[8]	0.84(3)
T4a	0.970(1)	0.0865(2)	0.22740(5)[9]	0.3766(4)[10]	0.84(3)
T4b	0.970(1)	−0.0877(2)	0.22740(5)[9]	0.3766(4)[10]	1.10(3)
O1a	0.970(1)	0.3778(1)[11]	−0.0845(1)[12]	0.1989(7)[13]	2.62(5)
O1b	0.970(1)	0.3778(1)[11]	−0.0845(1)[12]	0.5558(6)[14]	2.62(5)
O1c	0.970(1)	−0.3778(1)[11]	−0.0845(1)[12]	0.1989(7)[13]	2.62(5)
O1d	0.970(1)	−0.3778(1)[11]	−0.0845(1)[12]	0.5558(6)[14]	2.62(5)
O2a	0.970(1)	0.1224(1)[15]	0.1946(1)[16]	0.2021(7)[17]	2.1(1)
O2b	0.970(1)	0.1224(1)[15]	0.1946(1)[16]	0.5558(6)[14]	2.1(1)
O2c	0.970(1)	−0.1224(1)[15]	0.1946(1)[16]	0.2021(7)[17]	2.3(1)
O2d	0.970(1)	−0.1224(1)[15]	0.1946(1)[16]	0.5558(6)[14]	2.3(1)
O3a	0.970(1)	0.2380(1)[18]	0.1228(1)[19]	0.639(1)	3.04(7)
O3b	0.970(1)	0.2380(1)[18]	0.1228(1)[19]	0.119(1)	2.90(7)
O3c	0.970(1)	−0.2380(1)[18]	−0.1228(1)[19]	0.615(1)	3.04(7)
O3d	0.970(1)	−0.2380(1)[18]	−0.1228(1)[19]	0.142(1)	2.90(7)
O4a	0.970(1)	−0.3991(4)	−0.1960(3)	0.3578(9)	2.01(5)
O4b	0.970(1)	0.4015(4)	−0.1953(3)	0.3572(9)	2.05(7)
O5a	0.970(1)	0.1665(5)	0.1912(4)	0.876(1)	2.75(8)
O5b	0.970(1)	−0.1746(5)	0.1970(4)	−0.122(1)	2.75(8)
O6a	0.970(1)	0.3192(4)	0.0821(4)	0.3736(9)[20]	2.01(5)
O6b	0.970(1)	−0.3302(4)	0.0772(4)	0.3736(9)[20]	2.01(5)
O7a	0.970(1)	0.2700(4)	0.0014(3)[21]	0.1148(9)[22]	1.90(6)
O7b	0.970(1)	−0.2740(4)	0.0014(3)[21]	0.1148(9)[22]	1.90(6)
O8a	0.38(5)	0.244(1)	−0.256(1)	0.169(4)	2.4*
O8b	0.61(5)	0.2569(9)	−0.2435(8)	0.120(3)	2.4*
O8c	0.60(7)	0.2494(8)	−0.2570(6)	−0.399(3)	2.4*
O8d	0.39(7)	0.262(2)	−0.247(1)	−0.344(6)	2.4*
O9	0.970(1)	0.4999(5)	−0.0983(2)	0.386(1)	2.01(5)
O10	0.970(1)	0	0.2097(2)	0.379(2)	2.05(7)
T1Ba	0.029(1)	−0.30252(4)	−0.07286(9)	0.1683(3)	2.37*
T1Bb	0.029(1)	−0.30252(4)	0.07286(9)	0.0835(6)	2.37*
T1Bc	0.029(1)	0.30252(4)	−0.07286(9)	0.1683(3)	2.37*
T1Bd	0.029(1)	0.30252(4)	0.07286(9)	0.0837(3)	2.37*
T2Ba	0.029(1)	−0.19671(4)	−0.19037(9)	0.6698(4)	2.37*
T2Bb	0.029(1)	−0.19671(4)	−0.19037(9)	0.0789(3)	2.37*
T2Bc	0.029(1)	0.19671(4)	−0.19037(9)	−0.3304(3)	2.37*
T2Bd	0.029(1)	0.19671(4)	−0.19037(9)	0.0789(3)	2.37*
T3Ba	0.029(1)	−0.4132(2)	0.11776(5)	0.3743(4)	2.37*
T3Bb	0.029(1)	0.4122(2)	0.11776(5)	0.3743(4)	2.37*
T4Ba	0.029(1)	0.0877(2)	−0.22740(5)	0.3766(4)	2.37*
T4Bb	0.029(1)	−0.0865(2)	−0.22740(5)	0.3766(4)	2.37*
O1Ba	0.029(1)	−0.3778(1)	0.0845(1)	0.1989(7)	2.37*
O1Bb	0.029(1)	−0.3778(1)	0.0845(1)	0.5558(6)	2.37*
O1Bc	0.029(1)	0.3778(1)	0.0845(1)	0.5558(6)	2.37*
O1Bd	0.029(1)	0.3778(1)	0.0845(1)	0.1989(7)	2.37*
O2Ba	0.029(1)	−0.1224(1)	−0.1946(1)	0.2021(7)	2.37*
O2Bb	0.029(1)	−0.1224(1)	−0.1946(1)	0.5558(6)	2.37*
O2Bc	0.029(1)	0.1224(1)	−0.1946(1)	0.2021(7)	2.37*
O2Bd	0.029(1)	0.1224(1)	−0.1946(1)	0.5558(6)	2.37*
O3Ba	0.029(1)	−0.2380(1)	−0.1228(1)	0.639(1)	2.37*
O3Bb	0.029(1)	−0.2380(1)	−0.1228(1)	0.119(1)	2.37*
O3Bc	0.029(1)	0.2380(1)	0.1228(1)	0.615(1)	2.37*
O3Bd	0.029(1)	0.2380(1)	0.1228(1)	0.142(1)	2.37*

Table 3 (*continued*)

Atom	Population	x	y	z	B_{eq} [Å^2]
O4Ba	0.029(1)	0.3991(4)	0.1960(3)	0.3578(9)	2.37*
O4Bb	0.029(1)	0.1015(4)	−0.3053(3)	0.3572(9)	2.37*
O5Ba	0.029(1)	−0.1665(5)	−0.1912(4)	0.876(1)	2.37*
O5Bb	0.029(1)	0.1746(5)	−0.1970(4)	−0.122(1)	2.37*
O6Ba	0.029(1)	−0.3192(4)	−0.0821(4)	0.3736(9)	2.37*
O6Bb	0.029(1)	0.3302(4)	−0.0772(4)	0.3736(9)	2.37*
O7Ba	0.029(1)	−0.2700(4)	−0.0014(3)	0.1148(9)	2.37*
O7Bb	0.029(1)	0.2740(4)	−0.0014(3)	0.1148(9)	2.37*
O9B	0.029(1)	−0.4999(5)	0.0983(2)	0.386(1)	2.37*
O10B	0.029(1)	0	−0.2097(2)	0.379(2)	2.37*
Na1	0.66(1)	0.5002(8)	0.0006(6)	0.125(1)	4.1(1)
Na2	0.57(1)	0.001(1)	0.1845(5)	0.848(2)	7.90*
Na3	0.44(2)	0.0011(9)	0.1252(9)	0.647(2)	7.90*
W1	1.0	0.5005(8)	−0.0648(4)	0.877(2)	5.2(2)
W2	0.25(2)	0.000(3)	−0.174(3)	0.517(8)	7.90*
W3	0.42(1)	0.002(2)	0.092(1)	0.934(3)	7.90*
W5	0.55(2)	−0.545(1)	−0.189(1)	0.871(3)	7.90*
W11	0.29(2)	−0.504(2)	−0.217(2)	0.950(5)	7.90*
Se chain A					
A1	0.075(1)[a]	0.0570(9)	0.0198(9)	0.126(2)	3.48(8)*[g]
A2	0.075(1)[a]	0.1275(8)	−0.0184(8)	0.366(2)	3.48(8)*[g]
A3	0.075(1)[a]	0.0626(9)	0.0240(6)	0.611(1)	3.48(8)*[g]
A4	0.075(1)[a]	−0.0059(8)	−0.0675(6)	0.698(2)	3.48(8)*[g]
A5	0.075(1)[a]	−0.0059(8)	−0.0604(7)	0.007(2)	3.48(8)*[g]
A6	0.075(1)[a]	−0.102(1)	0.0146(8)	0.055(2)	3.48(8)*[g]
A7	0.075(1)[a]	−0.132(1)	−0.0066(9)	0.353(2)	3.48(8)*[g]
Se chain B					
B1	0.056(1)[b]	0.006(1)	0.0580(9)	0.364(3)	3.48(8)*[g]
B2	0.056(1)[b]	0.105(1)	−0.010(1)	0.438(2)	3.48(8)*[g]
B3	0.056(1)[b]	0.0994(9)	−0.007(1)	0.750(2)	3.48(8)*[g]
B4	0.056(1)[b]	−0.012(1)	−0.062(1)	0.800(2)	3.48(8)*[g]
B5	0.056(1)[b]	−0.0121(9)	−0.0711(8)	0.109(2)	3.48(8)*[g]
B6	0.056(1)[b]	−0.103(1)	0.005(1)	0.188(2)	3.48(8)*[g]
B7	0.056(1)[b]	−0.105(1)	−0.007(1)	0.498(2)	3.48(8)*[g]
Se chain C					
C1	0.027(1)[c]	0.091(2)	−0.003(3)	0.393(6)	3.48(8)*[g]
C2	0.027(1)[c]	0.037(2)	−0.047(2)	0.647(4)	3.48(8)*[g]
C3	0.027(1)[c]	−0.072(2)	0.014(2)	0.673(3)	3.48(8)*[g]
C4	0.027(1)[c]	−0.057(2)	0.063(1)	0.949(3)	3.48(8)*[g]
C5	0.027(1)[c]	−0.093(3)	−0.019(2)	0.145(4)	3.48(8)*[g]
C6	0.027(1)[c]	−0.12361	0.039(2)	0.400(3)	3.48(8)*[g]
Se chain D					
D1	0.041(1)[d]	0.092(2)	0.044(1)	0.293(2)	3.48(8)*[g]
D2	0.041(1)[d]	0.105(2)	−0.033(1)	0.517(2)	3.48(8)*[g]
D3	0.041(1)[d]	0.100(1)	0.033(1)	0.773(2)	3.48(8)*[g]
D4	0.041(1)[d]	0.0761(9)	−0.046(1)	0.991(2)	3.48(8)*[g]
D5	0.041(1)[d]	−0.0531(9)	−0.047(1)	0.997(2)	3.48(8)*[g]
D6	0.041(1)[d]	−0.075(1)	−0.0569(9)	0.303(2)	3.48(8)*[g]
D7	0.041(1)[d]	−0.096(2)	0.052(1)	0.383(3)	3.48(8)*[g]
Se chain E					
E1	0.030(1)[e]	−0.065(1)	−0.036(2)	0.533(4)	3.48(8)*[g]
E2	0.030(1)[e]	0.063(1)	−0.045(2)	0.560(3)	3.48(8)*[g]
E3	0.030(1)[e]	0.087(1)	0.019(1)	0.811(3)	3.48(8)*[g]
E4	0.030(1)[e]	0.044(2)	−0.048(1)	0.041(3)	3.48(8)*[g]
E5	0.030(1)[e]	−0.064(2)	0.008(2)	0.125(3)	3.48(8)*[g]
E6	0.030(1)[e]	−0.104(2)	−0.056(1)	0.365(3)	3.48(8)*[g]
E7	0.030(1)[e]	−0.108(2)	0.021(2)	0.594(3)	3.48(8)*[g]
Se chain F					
F1	0.074(1)[f]	0.102(1)	0.0031(9)	0.054(2)	3.48(8)*[g]
F2	0.074(1)[f]	0.1120(6)	0.0194(9)	0.363(2)	3.48(8)*[g]

(*continued on next page*)

Table 3 (*continued*)

Atom	Population	x	y	z	B_{eq} [Å^2]
F3	0.074(1)[f]	−0.0083(7)	0.0508(7)	0.434(2)	3.48(8)*[g]
F4	0.074(1)[f]	−0.0467(8)	−0.0385(6)	0.613(1)	3.48(8)*[g]
F5	0.074(1)[f]	−0.1056(9)	0.0174(9)	0.846(1)	3.48(8)*[g]
F6	0.074(1)[f]	−0.0561(9)	−0.0375(7)	0.094(1)	3.48(8)*[g]
F7	0.074(1)[f]	−0.1038(9)	0.0270(9)	0.327(2)	3.48(8)*[g]
Various Se atoms					
G1	0.095(3)	0.0962(9)	0.0041(8)	0.678(2)	3.48(8)*[g]
G2	0.128(4)	−0.1084(6)	0.0078(6)	0.910(2)	3.48(8)*[g]
G3	0.101(3)	−0.0980(7)	−0.0080(7)	0.252(2)	3.48(8)*[g]
G4	0.036(2)	0.002(2)	−0.069(1)	0.216(4)	3.48(8)*[g]

[1–22]Coordinates with the same superscript were constrained to be equal. All atomic parameters (coordinates, population, isotropic displacement factors) labeled B are fully constrained and belong to a domain of mordenite shifted $c/2$ relative to the main part of the structure [27]. [a–g]Parameters of the Se-sites with the same superscript were constrained to be equal.

* Starred atoms with standard deviation were refined isotropically, those without standard deviations were fixed. Anisotropically refined atoms are given in the form of the isotropic equivalent thermal parameter defined as $B_{eq} = 8/3\ \pi^2 \sum_i (\sum_j (U_{ij} a_i^* a_j^* a_i \cdot a_j))$.

Table 4
T–O distances (Å) of Se-mordenite-Na with standard deviations in parentheses

Bond		Bond		Bond	
T1a–O6a	1.592(7)	T2a–O3a	1.604(3)	T3a–O4b	1.600(7)
T1a–O3b	1.595(3)	T2a–O2b	1.601(4)	T3a–O1a	1.620(5)
T1a–O1b	1.620(3)	T2a–O8 (ave)	1.61(1)	T3a–O9	1.630(9)
T1a–O7a	1.614(7)	T2a–O5a	1.630(9)	T3a–O1b	1.652(5)
Mean	1.605	Mean	1.612	Mean	1.625
T1b–O3a	1.604(3)	T2b–O3b	1.603(3)	T3b–O1d	1.615(5)
T1b–O6a	1.618(7)	T2b–O5a	1.630(9)	T3b–O4a	1.630(8)
T1b–O1a	1.626(3)	T2b–O2a	1.626(4)	T3b–O9	1.629(9)
T1b–O7a	1.662(7)	T2b–O8 (ave)	1.66(1)	T3b–O1c	1.646(5)
Mean	1.627	Mean	1.631	Mean	1.630
T1c–O1c	1.621(3)	T2c–O8 (ave)	1.58(1)	T4a–O4a	1.599(7)
T1c–O7b	1.576(7)	T2c–O2d	1.602(4)	T4a–O2a	1.628(5)
T1c–O3c	1.612(3)	T2c–O3d	1.594(3)	T4a–O10	1.596(3)
T1c–O6b	1.631(7)	T2c–O5b	1.611(9)	T4a–O2b	1.630(4)
Mean	1.610	Mean	1.596	Mean	1.613
T1d–O7b	1.626(7)	T2d–O5b	1.568(9)	T4b–O2c	1.610(5)
T1d–O1d	1.632(3)	T2d–O3c	1.598(3)	T4b–O4b	1.624(7)
T1d–O6b	1.649(7)	T2d–O2c	1.625(4)	T4b–O10	1.638(3)
T1d–O3d	1.620(3)	T2d–O8 (ave)	1.60(1)	T4b–O2d	1.613(4)
Mean	1.632	Mean	1.597	Mean	1.621

in mordenite-Na, whereas the Na3 position situated in the 12-membered ring channel, is significantly lower occupied in Se-mordenite-Na. This can be explained by a partial displacement of Na by the Se chains and the partially dehydrated status of Se-mordenite-Na.

3.2. Raman spectroscopy

Se incorporated under different conditions and in different types of mordenite has been widely investigated by Raman spectroscopy [9–15]. Prominent vibration bands in Se-modified mordenites lie between 200 and 300 cm^{-1}. Raman spectra of Se-mordenite-Na can be compared with the vibration spectra of elemental Se. The most active Raman band in helical, trigonal Se is the A1 symmetric stretching mode at 237 cm^{-1}, which strongly depends on chain interactions [29]. The most dominant vibrational band in our Se-mordenite-Na was detected at 254 cm^{-1}. According to the literature, the 254 cm^{-1} band in Se-mordenite-Na can be attributed to the A1 symmetric stretching mode in elemental trigonal Se [9–15]. The difference between the A1 mode of elemental Se and Se in mordenite can be interpreted as interaction of Se with channel wall atoms, but also as a missing chain interaction in Se-mordenite-Na because the single chains are laterally separated through the mordenite channels. Bands characteristic of other forms than chains, e.g. Se_6 or Se_8 rings, were not observed.

Table 5
T–O distances (Å) of mordenite-Na with standard deviations in parentheses

Bond		Bond		Bond	
T1a–O6a	1.614(6)	T2a–O3a	1.604(2)	T3a–O4b	1.632(7)
T1a–O3b	1.614(3)	T2a–O2b	1.594(3)	T3a–O1a	1.617(6)
T1a–O1b	1.629(4)	T2a–O8 (ave)	1.612(8)	T3a–O9	1.644(7)
T1a–O7a	1.593(6)	T2a–O5a	1.595(7)	T3a–O1b	1.667(5)
Mean	1.613	Mean	1.601	Mean	1.640
T1b–O3a	1.602(3)	T2b–O3b	1.595(3)	T3b–O1d	1.597(5)
T1b–O6a	1.649(6)	T2b–O5a	1.658(7)	T3b–O4a	1.598(5)
T1b–O1a	1.652(5)	T2b–O2a	1.623(3)	T3b–O9	1.617(7)
T1b–O7a	1.621(6)	T2b–O8 (ave)	1.612(8)	T3b–O1c	1.658(5)
Mean	1.631	Mean	1.622	Mean	1.618
T1c–O1c	1.583(5)	T2c–O8 (ave)	1.612(8)	T4a–O4a	1.636(5)
T1c–O7b	1.621(6)	T2c–O2d	1.594(3)	T4a–O2a	1.625(4)
T1c–O3c	1.614(3)	T2c–O3d	1.596(3)	T4a–O10	1.580(2)
T1c–O6b	1.596(6)	T2c–O5b	1.574(7)	T4a–O2b	1.654(4)
Mean	1.603	Mean	1.594	Mean	1.624
T1d–O7b	1.626(6)	T2d–O5b	1.613(7)	T4b–O2c	1.591(4)
T1d–O1d	1.616(5)	T2d–O3c	1.589(3)	T4b–O4b	1.590(7)
T1d–O6b	1.630(6)	T2d–O2c	1.625(3)	T4b–O10	1.660(3)
T1d–O3d	1.649(3)	T2d–O8 (ave)	1.611(8)	T4b–O2d	1.621(4)
Mean	1.630	Mean	1.610	Mean	1.615

Our results from Raman spectroscopy are completely consistent with other spectroscopy studies according to incorporation conditions, methods, and used mordenite samples. The results clearly suggest a chain like arrangement of incorporated Se. Compared to the sharp 237 cm^{-1} stretching mode in trigonal Se [30], the 254 cm^{-1} band of Se-mordenite-Na is strongly broadened. This broadening can be interpreted as an overlay due to Se chains with different geometries. To check the existence of SeO species (SeO_2, selenites, selenates), the Raman spectra of Se-mordenite-Na was compared with Se–O stretching modes as they occur in SeO species. The vibrational behaviour of SeO_2 is well established [31] and shows prominent modes between 500 and 900 cm^{-1}. Our Raman spectra displays no bands in this region. Therefore, it can be concluded to that no moieties containing Se–O bonds are present in the structure.

3.3. Se atoms

Six chains (all only partly occupied) consisting of up to seven Se atoms were found, all located in the large 12-membered ring channel along the *c*-axis. Because 1st neighbor and 2nd neighbor distances in Se chains are well established, these distances were fixed to 2.34 Å (1st neighbor) and 3.62 Å (2nd neighbor) [17–19], resulting in bond angles of 102°. Such constrains were necessary to handle the overlay of partly occupied chain fragments. Distances of 3rd and further neighbors were not fixed resulting in bonds of different lengths (4–6 Å to the 3rd neighbor) and different dihedral angles. The population was constrained to be equal within a chain, and isotropic displacement parameters were constrained to be equal for all Se atoms.

Chain A has a length of 9.85 Å and is made up of seven Se atoms. The chain has a total population of 2.1 Se p.f.u. The closest distance to channel oxygen is 3.14 Å from Se atom A7 to O7b. Third neighbor distances are A1–A4 4.79 Å, A2–A5 5.45 Å, A3–A6 4.47 Å and A4–A7 5.56 Å with torsion angles of 99.4° (A1–A2–A3–A4), 142.9° (A2–A3–A4–A5), 81.8° (A3–A4–A5–A6) and 159.8° (A4–A5–A6–A7).

Chain B contains also seven Se atoms and is 8.84 Å long with a total population of 1.8 Se p.f.u. The shortest distance to the channel wall is between Se at B4 and O10 with 3.08 Å. Third neighbor distances are B1–B4 4.10 Å, B2–B5 5.62 Å, B3–B6 4.93 Å and B4–B7 5.61 Å with torsion angles of 67.3° (B1–B2–B3–B4), 172.9° (B2–B3–B4–B5), 107.1° (B3–B4–B5–B6) and 178.4° (B4–B5–B6–B7).

Se chain C consists of six atoms with a length of 8.5 Å and has a low occupancy of 0.6 Se p.f.u. The closest framework oxygen is O3d to C6 with a distance of 3.24 Å. Third neighbor distances are C1–C4 5.117 Å, C2–C5 4.48 Å and C3–C6 5.57 Å with torsion angles of −112.6° (C1–C2–C3–C4), −75.6° (C2–C3–C4–C5) and −147.5° (C3–C4–C5–C6).

Chain D with seven Se atoms has a length of 8.9 Å and is populated with 1.12 Se p.f.u. Closest distance to channel oxygen is 3.12 Å from Se atom D2 to O3b. Third neighbor distances are D1–D4 5.57 Å, D2–D5 4.61 Å, D3–D6 5.41 Å and D4–D7 4.73 Å with torsion angles of 163.1° (D1–D2–D3–D4), −90.9° (D2–D3–D4–

D5), −140.2° (D3–D4–D5–D6) and 97.5° (D4–D5–D6–D7).

Chain E has a length of 8.1 Å and a low occupancy of 0.84 Se p.f.u. O7b is nearest to E7 with a bond length of 3.04 Å. Third neighbor distances are E1–E4 4.3 Å, E2–E5 4.94 Å, E3–E6 5.62 Å and E4–E7 5.18 Å with torsion angles of 73.7° (E1–E2–E3–E4), −107.7° (E2–E3–E4–E5), −176.9° (E3–E4–E5–E6) and 121.8° (E4–E5–E6–E7).

Chain F is the longest chain with 10.3 Å and has a high population of 2.1 p.f.u. F1 is closely located to O7a (3.07 Å). Third neighbor distances are F1–F4 5.06 Å, F2–F5 5.35 Å, F3–F6 5.35 Å and F4–F7 5.63 Å with torsion angles of 113.8° (F1–F2–F3–F4), 136.2° (F2–

Table 6
Chain lengths (Å), 3rd neighbor distances (Å) and torsion angles (°) of Se chains

Atom 1	Atom 2	Distance	Atom 1	Atom 2	Atom 3	Atom 4	Angle
Third neighbor			*Torsion angle*				
A1	A4	4.80(2)	A1	A2	A3	A4	99.415(7)
A2	A5	5.46(2)	A2	A3	A4	A5	142.908(6)
A3	A6	4.47(2)	A3	A4	A5	A6	81.796(9)
A4	A7	5.57(2)	A4	A5	A6	A7	159.746(4)
Chain length							
A1	A7	9.85(2)					
Third neighbor			*Torsion angle*				
B1	B4	4.11(3)	B1	B2	B3	B4	67.342(9)
B2	B5	5.62(2)	B2	B3	B4	B5	172.961(1)
B3	B6	4.93(3)	B3	B4	B5	B6	107.146(9)
B4	B7	5.62(2)	B4	B5	B6	B7	178.421(2)
Chain length							
B1	B7	8.85(3)					
Third neighbor			*Torsion angle*				
C1	C4	5.12(5)	C1	C2	C3	C4	−112.606(1)
C2	C5	4.48(5)	C2	C3	C4	C5	−75.639(7)
C3	C6	5.56(4)	C3	C4	C5	C6	147.487(5)
Chain length							
C1	C6	8.54(5)					
Third neighbor			*Torsion angle*				
D1	D4	5.57(3)	D1	D2	D3	D4	163.132(3)
D2	D5	4.61(3)	D2	D3	D4	D5	−90.874(8)
D3	D6	5.41(3)	D3	D4	D5	D6	−140.340(4)
D4	D7	4.73(3)	D4	D5	D6	D7	97.531(2)
Chain length							
D1	D7	8.87(3)					
Third neighbor			*Torsion angle*				
E1	E4	4.30(4)	E1	E2	E3	E4	73.686(8)
E2	E5	4.94(3)	E2	E3	E4	E5	−107.649(9)
E3	E6	5.62(4)	E3	E4	E5	E6	−176.911(7)
E4	E7	5.18(4)	E4	E5	E6	E7	121.863(7)
Chain length							
E1	E7	8.10(4)					
Third neighbor			*Torsion angle*				
F1	F4	5.06(2)	F1	F2	F3	F4	113.806(6)
F2	F5	5.35(2)	F2	F3	F4	F5	136.173(7)
F3	F6	5.35(2)	F3	F4	F5	F6	−134.121(5)
F4	F7	5.63(2)	F4	F5	F6	F7	173.326(8)
Chain length							
F1	F7	10.27(2)					

First and second neighbor distances and bond angle are not displayed because they were fixed during refinement. Corresponding mean bond lengths and angle are 2.34(3) (1st neighbor), 3.62(2) (2nd neighbor) and 102(1)° (bond angle).

F3–F4–F5), −134.1° (F3–F4–F5–F6) and 173.3° (F4–F5–F6–F7). Four additional low occupied Se positions were located in the 12-membered ring channel but could not be assigned to a chain. Distances and angles are summarized in Table 6.

4. Discussion

4.1. H_2O in Se-loaded mordenite-Na

Dehydration of natural and cation exchanged mordenites is widely discussed in the literature [32–36]. The framework of mordenite shows almost no lattice deformation upon dehydration. Total water loss in natural mordenite was predicted at 300 °C [33], for mordenite-Ca at 500 °C, respectively [34]. The H_2O site, which is most resistant to dehydration, coordinates the extraframework cations within the compressed 8-membered ring channels. In natural mordenite Ca usually occupies this site [27], which bonds considerably stronger to H_2O than Na in our synthetic mordenite-Na. This explains the lower dehydration temperature (≈280 °C) for mordenite-Na. Compared to mordenite-Na (19 H_2O p.f.u., Fig. 5), 10 H_2O molecules p.f.u. were detected in Se-mordenite-Na. This H_2O content can be explained by rehydration due to subsequent storage of the sample at ambient humidity conditions. Even if the large channels are plugged by Se chains, H_2O molecules find appropriate diffusion pathways along the compressed 8-membered ring channels along *b* and *c*. A reaction of this re-incorporated H_2O and Se within the structure at ambient conditions cannot be expected. The H_2O molecules in Se-mordenite-Na are located at five different sites: (1) a highly populated position in the 8-membered ring channel along *c*, which is coordinated to Na1; (2) two positions in the 8-membered ring channel along *b*; (3) two positions in the 12-membered ring channel along *c* close to the Na2 and Na3 positions (Fig. 6).

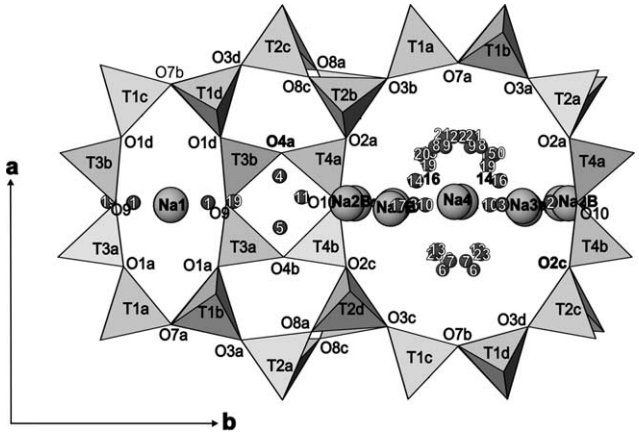

Fig. 5. Extraframework cation and H_2O molecule positions in mordenite-Na. Small circles with numbers correspond to H_2O positions.

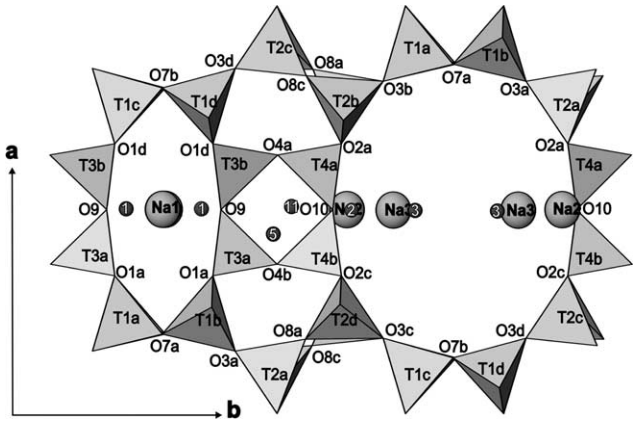

Fig. 6. Extraframework cation and H_2O molecule positions in Se-mordenite-Na. Small circles with numbers correspond to H_2O positions. Se positions are not displayed.

4.2. The mordenite framework

The mordenite structure at room temperature is usually refined in space group *Cmcm* or $Cmc2_1$, respectively [1,28]. Simoncic and Armbruster [27] proposed a domain like structure where about 3% of the Si/Al framework is shifted by $c/2$. In spite of these studies, the symmetry of the framework is generally handled as pseudosymmetry and represents only a fair approximation. Lower symmetries or micro-twin models are also supposed [37] but not proven by experiments. Several space groups were tested during structural refinement: orthorhombic *Cmcm* and $Cmc2_1$, and monoclinic $C2/c$ and *Cc*. For mordenite-Na and Se-mordenite-Na at 120 K the space group *Cc* represents the most suitable model. Because the *Cc* model fits both structures, it can be ruled out that a phase transition from $Cmc2_1$ to *Cc* occurred due to Se incorporation.

Application of low temperature (120 K), chosen for an improved resolution of extraframework occupants, led also to a better resolution of the complex disordered microstructure within the tetrahedral framework [37]. However, we were not able to develop a correct intergrowth/twinning model for the description of the tetrahedral framework. After refinements in space group *Cmcm* and $Cmc2_1$ indicated only poor agreement between structure model and diffraction data, we have chosen as a "best" compromise the monoclinic space group *Cc*. Furthermore, to reduce correlation problems due to pseudosymmetry, related tetrahedral sites and their atomic displacement parameters were constrained to each other. As will be shown below, Se chains may be longer than the periodicity of the framework parallel to the channel axis. The fact that we did not observe any superstructure reflection or diffuse scattering evidence for the Se-treated mordenite-Na, different to mordenite-Na, indicates that the distribution of Se chains along the *c*-axis is rather random.

4.3. Arrangement of Se atoms in mordenite

For a better understanding of Se arrangement in mordenite, it is important to discuss some principal geometrical features of Se chains. In a chain of atoms A–B–C–D, the torsion angle or dihedral angle is defined as the angle between the plane containing the atoms A, B, C and that containing B, C, D, having an absolute value between 0° and 180° (Fig. 7). Positive torsion angles are oriented clockwise, negative angles counter clockwise. Minimal 3rd neighbor distance results from a torsion angle of 0°, which is the energetically most unfavorable conformation, whereas maximal 3rd neighbor distance results from a torsion angle of 180°. For comparison, the torsion angle in trigonal helical Se is ideally 101° with a 3rd neighbor distance of 4.95 Å, which corresponds to the *c*-axis of the unit cell of this modification [7]. 101° is for trigonal Se the energetically most favorable dihedral angle because of repulsion between non-bonding lone-pair electrons on the adjacent Se atoms in the chain [19]. Most studies concerning Se incorporated into mordenite investigated short-range order and bonding of the Se atoms. Therefore the 1st and 2nd neighbor distances in mordenite Se chains are well established, but the 3rd neighbor distance and torsion angle are difficult to determine with spectroscopic methods and rather controversial models were proposed. The dihedral angle is crucial for the geometry of the Se chain because it represents the "softest" structural parameter with the highest rotational potential.

In our refinement we arranged six Se chains, each with different geometry related to torsion angles and 3rd neighbor distances. 7.9 Se p.f.u. were determined analytically by electron microprobe, but 10.04 Se p.f.u. were obtained from structure refinement. The excess of refined Se may be explained by disorder of Se chains, and possible overlay with extraframework Na and H_2O, or even due to Se loss under the electron beam of the electron microprobe. Torsion angles within the chains differ between |67°| and |180°|, which deviate clearly from the value in trigonal Se. Third neighbor distances range between 4.11(3) and 5.63(2) Å.

The arrangement in the refined Se chains can be simplified by introducing two idealized geometrical conformations: (1) torsion angle < 160° resulting in a staggered arrangement of four coherent Se atoms, similar to the conformation in trigonal Se; (2) torsion angle > 160° resulting in a planar, zigzag-shaped arrangement of four coherent Se atoms (Fig. 8). These two conformations appear side by side in the Se chains, which is shown in Figs. 9 and 10 for chains B and F. The zigzag-like geometry corresponds to the chains calculated by the semiempirical models of Ikawa and Fukutome [20,21]. They showed that Se chain geometries with dihedral angles between 70° and 180° are possible. Although a planar arrangement disagrees with the torsion angle in trigonal Se, this can be interpreted [20,21] as chain defects due to the influence of channel cations or H_2O molecules.

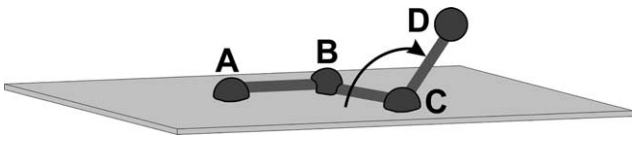

Fig. 7. Torsion angle within a group of four atoms A–B–C–D: A torsion angle is defined as the angle from the plane built by atoms A, B and C to atom D. Positive angles are clockwise oriented, negative angles counter clockwise.

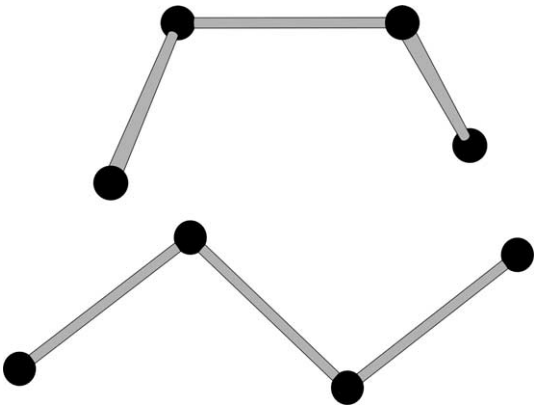

Fig. 8. Staggered arrangement with dihedral angle < 160°. Planar arrangement with dihedral angle > 160°.

Katayama et al. [19] used results from EXAFS to derive 1st, 2nd and 3rd neighbor distances as well as bond- and dihedral angle and postulated that the helical chain form is preserved. However, the uniform dihedral angle of 74° and 3rd neighbor distance of 4.32(4) as principal structure parameters for a Se chain in mordenite cannot be confirmed by our refinements.

Porbochii [10] proposed, based on Raman spectroscopy, a uniformly shaped Se chain formed by *cis*- and *trans*-segments. These segments consist of two different

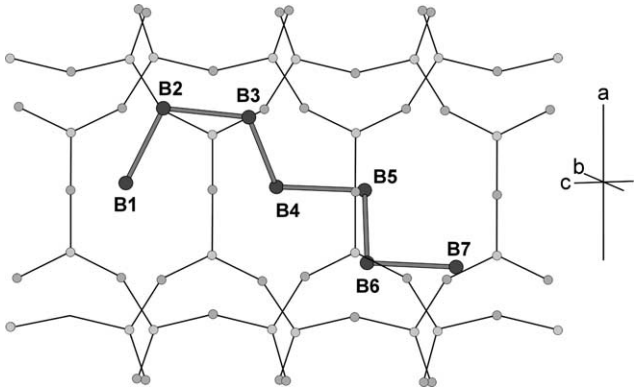

Fig. 9. Chain B: Atoms B1–B2–B3–B4 (67°) and B3–B4–B5–B6 (107°) build a staggered geometry whereas B2–B3–B4–B5 (173°) and B4–B5–B6–B7 (178°) have a zigzag geometry.

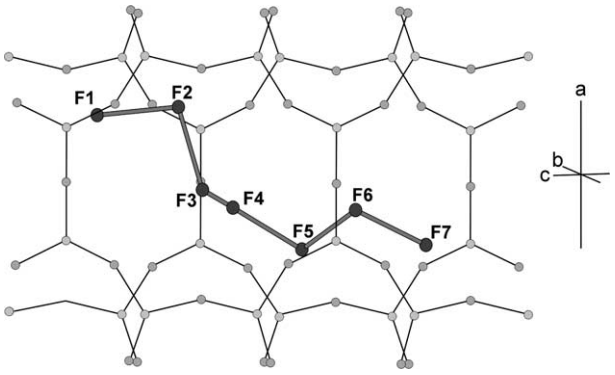

Fig. 10. Torsion angle from atom groups F1–F2–F3–F4, F2–F3–F4–F5 and F3–F4–F5–F6 have all staggered geometry, only F4–F5–F6–F7 has zigzag geometry.

bond lengths (1st neighbor distances) and two different bond angles with varying negative and positive dihedral angle of |90°|. This Se arrangement cannot be supported by our study or by other spectroscopic studies where the 1st neighbor distances were clearly determined at 2.34 Å. The study of Bogomolov et al. [8] supports our suggestion that the Se chain in mordenite differs from trigonal Se and shows variable geometry. Due to the influence of framework atoms and the symmetry-superposition principle, they concluded that Se chains located in the mordenite channel has not the symmetry of trigonal Se as the dihedral angle of the Se chain varies randomly.

The Se chain geometry is also influenced by adjacent framework oxygen. Closest distances between a chain atom and a framework oxygen range from 3.04 to 3.24 Å. This is longer than the covalent Se–O bond length (1.624, 1.795 Å, respectively) in SeO_2 [38], but shorter than the sum of the van der Waals radii of Se and O (3.42 Å). Thus there is a slight electrostatic interaction between the Se atom and the adjacent oxygen of the framework.

Other Se species like Se_6 and even Se_8 rings were postulated by Poborchii and co-authors [11,12]. The latter authors compared Raman spectra of Se-mordenite-Na and trigonal as well as monoclinic elemental Se and postulated the existence of chains and rings in the 12-membered ring channel of mordenite. In our study Se_6 or Se_8 rings were neither confirmed by structure refinement nor by Raman spectroscopy. Poborchii et al. [13] investigated also the dependence of type of extra-framework cations on the concentration of Se species, observing higher concentrations of Se_6 rings in mordenite-K than in mordenite-Na.

Because of electrostatic interactions between Se chains and framework, influence of disordered channel cations and H_2O molecules, the Se chains display variable forms. Furthermore, due to residual Se positions in the difference Fourier map, the proposed refined arrangement of Se chains can only be taken as a fair approximation to the real chain geometry. However, regular chain geometry as in trigonal Se cannot be confirmed by our data. Strong disorder of the Se arrangement has to be supposed and no prediction can be made about the real length of a Se chain. Summarizing it must be concluded that Se chains in mordenite are not uniform, but show highly variable geometrical arrangement.

Acknowledgements

This study was supported by the Swiss "Nationalfond", credit 20-65084.01 to T. Armbruster. We acknowledge the European Synchrotron Radiation Facility for provision of synchrotron radiation facilities and we would like to thank V. Dmitriev for assistance in using the Swiss–Norwegian beam line 1A. We thank E. Gnos for chemical analyses with the electron microprobe and B. Frey for crystal images by SEM and TG analysis.

References

[1] V.V. Poborchii, A.V. Kolobov, J. Caro, V.V. Zhuravlev, K. Tanaka, Chem. Phys. Lett. 280 (1997) 17.
[2] A. Goldbach, L. Iton, M.-L. Saboungi, Chem. Phys. Lett. 281 (1997) 69.
[3] V.V. Poborchii, J. Chem. Phys. 114 (6) (2001) 2702.
[4] W.M. Meier, Zeit. Kristall. 115 (1961) 439.
[5] W.M. Meier, in: L.B. Sand, F.A. Mumpton (Eds.), Natural Zeolites, Occurrence, Properties, Use, 1978, p. 99.
[6] T. Armbruster, M.E. Gunter, in: D.L. Bish, D.W. Ming (Eds.), Natural Zeolites: Occurrence, Properties, Use, in: Reviews in Mineralogy & Geochemistry, vol. 45, 2002, p. 1.
[7] P. Cherin, P. Unger, Inorg. Chem. 6 (8) (1967) 1589.
[8] V.N. Bogomolov, S.V. Kholodkevich, S.G. Romanov, L.S. Agroskin, Solid State Comm. 47 (3) (1983) 181.
[9] V.N. Bogomolov, V.V. Poborchii, S.G. Romanov, S.I. Shagin, J. Phys. C: Solid State Phys. 18 (1985) 313.
[10] V.V. Poborchii, J. Phys. Chem. Solids 55 (8) (1994) 737.
[11] V.V. Poborchii, Chem. Phys. Lett. 251 (1996) 230.
[12] V.V. Poborchii, A.V. Kolobov, H. Qyanagi, S.G. Romanov, K. Tanaka, Chem. Phys. Lett. 280 (1997) 10.
[13] V.V. Poborchii, A. Kolobov, H. Oyanagi, S. Romanov, K. Tanaka,, Nanostruct. Mat. 10 (3) (1998) 427.
[14] V.V. Poborchii, Solid State Comm. 107 (9) (1998) 513.
[15] V.V. Poborchii, A.V. Kolobov, J. Caro, V.V. Zhuravlev, K. Tanaka, Phys. Rev. Lett. 82 (9) (1999) 1955.
[16] O. Terasaki, K. Yamazaki, J.M. Thomas, T. Ohsuna, D. Watanabe, J.V. Sanders, J.C. Barry, J. Solid State Chem. 77 (1988) 72.
[17] L. Khouchaf, M.-H. Tuilier, J.L. Guth, B. Elouadi, J. Phys. Solids. 57 (5) (1996) 251.
[18] J.B. Parise, J.E. Mac Dougall, N. Herron, R. Farlee, A.W. Sleight, Y. Wang, T. Bein, K. Möller, L.M. Moroney, Inorg. Chem. 27 (1988) 221.
[19] Y. Katayama, M. Yao, Y. Ajiro, M. Inui, H. Endo, J. Phys. Soc. Jap. 58 (5) (1989) 1811.
[20] A. Ikawa, H. Fukutome, J. Phys. Soc. Jap. 58 (12) (1989) 4517.
[21] A. Ikawa, H. Fukutome, J. Phys. Soc. Jap. 59 (3) (1990) 1002.
[22] J. Warzywoda, A.G. Dixon, R.W. Thompson, A. Sacco Jr., J. Mat. Chem. 5 (7) (1995) 1019.

[23] P. Simoncic, T. Armbruster, in: P. Misaelides (Ed.), Zeolite'02, 6th International Conference on the Occurrence, Properties and Utilization of Natural Zeolites, 2002, p. 336.
[24] Oxford Diffraction Xcalibur System, User Manual, CrysAlis Software Package, version 1.169, Oxfordshire, UK, 2001.
[25] G.M. Sheldrick, SADABS, version 2.06, Empirical Absorption Correction Program, University of Göttingen, Germany, 2002.
[26] G.M. Sheldrick, SHELX-97, University of Göttingen, Germany, 1997.
[27] P. Simoncic, T. Armbruster, Am. Mineral. 89 (2004) 421.
[28] A. Alberti, P. Davoli, P.G. Vezzalini, Zeit. Kristall. 175 (1986) 249.
[29] G. Lucovsky, A. Mooradian, W. Taylor, G.B. Wright, Solid State Comm. 5 (1967) 113.
[30] M.H. Brodsky, in: M. Cardona (Ed.), Light Scattering in Solids, Springer, Berlin, 1975, p. 208.
[31] A. Anderson, A. Sanders, W. Smith, J. Raman Spec. 31 (2000) 403.
[32] L.P. van Reeuwijk, The Thermal Dehydration of Natural Zeolites, Ph.D. Thesis, Landbouwhogeschool Wageningen, 1974, p. 22.
[33] A. Gottardi, E. Galli, Natural Zeolites, Springer, Berlin, 1985, p. 223.
[34] J. Elsen, G.S.D. King, W.J. Mortier, J. Phys. Chem. 91 (1987) 5800.
[35] A. Martucci, M. Sacerdoti, G. Cruciani, Surf. Sci. Catal. 135 (2001) 290.
[36] A. Martucci, M. Sacerdoti, G. Cruciani, C. Dalconi, Eur. J. Mineral. 15 (2003) 485.
[37] R. Gramlich-Meier, Strukturparameter in Zeolithen der Mordenitfamilie, Dissertation ETH Zürich, Nr. 6760 (1981).
[38] K. Stahl, J.P. Legros, J. Galy, Zeit. Kristall. 202 (1992) 99.